ChemComm

Accepted Manuscript

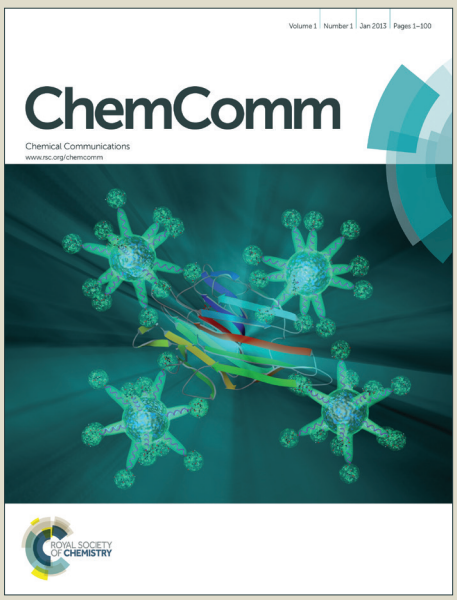

ROYAL SOCIETY OF CHEMISTRY

www.rsc.org/chemcomm

Journal Name

COMMUNICATION

Core-shell hierarchical WO_2/WO_3 microsphere as an electrocatalyst support for methanol electrooxidation

Received 00th January 20xx,
Accepted 00th January 20xx

DOI: 10.1039/x0xx00000x

www.rsc.org/

Yang Zhou,*[a] Xian-Chao Hu, [b] Xi-Hui Liu, [a] and He-Rui Wen*[a]

The core-shell WO_2/WO_3 microspheres were prepared by the phase transformation route. The as-prepared Pt-WO_2/WO_3 catalyst exhibits excellent activity and stability towards methanol electrooxidation compared with that of the commercial PtRu/C and Pt/h-WO_3 due to the decrease of the electron-transfer resistance by the modification of WO_2 as a conductive oxide.

Tungsten trioxide (WO_3) has attracted considerable attention in recent years, mainly due to its insolubility in acid solution and special electrochemical property, especially for direct methanol fuel cell (DMFC) application. [1] It is well known that this material can form tungsten bronzes compound to facilitate the dehydrogenation of methanol, and also the oxophilic nature of oxide favors to remove the adsorbed intermediates during the methanol electrooxidation (MOR). Numerous studies demonstrated that Pt or PtRu supported on WO_3 had excellent catalytic activity towards the electrooxidation of carbon monoxide,[2] methanol[3] and formic acid.[4] Unfortunately, WO_3 has a low specific surface area and electric conductivity, which limits its application in the DMFC.

Several shape-controlled WO_3 including nest-like-porous, [5] three-dimensionally ordered macroporous [6] and microsphere [7] have recently been reported to increase the specific surface area. Along with the specific surface area and corrosion resistance, the electric conductivity is also an extremely important characteristic with regard to electrocatalysts support. Nevertheless, it is still a great challenge to enhance electronic conductivity of WO_3 because WO_3 is an n-type semiconductor with a reported band gap of about 2.6 to 2.8 eV.

Among transition metal oxides, tungsten trioxide (WO_2) possesses metallic conductivity (the electronic conductivity is about 3.5×10^2 S cm^{-1}) due to oxygen vacancy defects in the lattice and the strong metal-metal bonding inherent to the crystal structure of WO_2.[8] Previous research demonstrated that the modification of WO_2 could enhance the electrochemical performances of $LiFePO_4$/C cathode material for lithium-ion batteries because the existence of WO_2 as a conductive oxide improves the discharge specific capability and decreases charge transfer resistance.[9] Herein, we report an efficient synthesis of the core-shell WO_2/WO_3 microspheres via phase transformation route on the basis of WO_3 microspheres previously prepared by spray drying reported by our group.[10] It is expected that the core-shell WO_2/WO_3 microspheres will exhibit better electrical conductivity than WO_3 microspheres, which is beneficial to the electrochemical properties of catalyst supported on the WO_2/WO_3. Furthermore, the method above mentioned can also be extended to the synthesis of other metal oxide/carbide with the core-shell hierarchical structure.

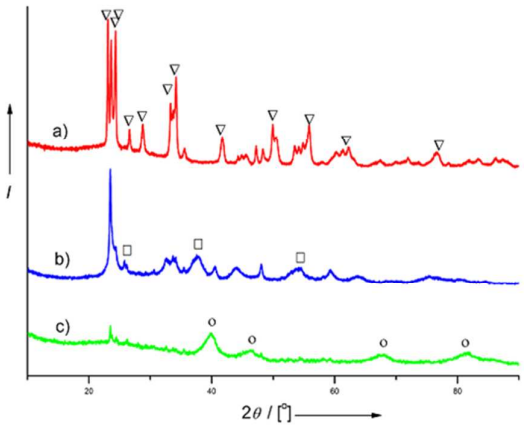

Fig. 1 XRD patterns of a) h-WO_3, b) WO_2/WO_3, c) Pt-WO_2/WO_3 ▽ WO_3, □ WO_2, ○ Pt

The entire synthetic process for preparing Pt-WO_2/WO_3 catalyst is schematically depicted in Figure S1 in the Supporting Information. The hollow ammonium metatungstate microsphere (HAMT) precursor was first fabricated by spray-drying method. The core-shell hierarchical WO_2/WO_3 microspheres were then prepared by in situ reducing HAMT under atmosphere of CO and CO_2. Finally, Pt nanoparticles were reduced and deposited on the surface of WO_2/WO_3.

Hollow tungsten trioxide spheres (h-WO_3) were also synthesized by spay drying method combined with proper calcinations(Figure S2). The typical XRD pattern of h-WO_3 is

shown in Figure 1a. It can be found that all of the diffraction peaks of h-WO_3 can be indexed to pure monoclinic WO_3 (JCPDS card no. 043-1035), indicating well-crystallized WO_3 framework. Thermogravimetric analysis (TGA) results of the as-prepared WO_2/WO_3 support in air are shown in Figure 2. From 18 °C to 135 °C, the total weight loss is 0.5 %, which is due to dehydration. The WO_2 phase begins to transform into WO_3 at an elevated temperature (>135 °C). From 135 °C to 570 °C, the total weight increase is 6.5 %, which is close to the reaction:

$2WO_2 + O_2 \longrightarrow 2WO_3$ ($\triangle$m = 7.4 %, referenced to WO_2) (1)

There is a strong exothermal peak at around 426 °C, which should be attributed to the oxidation reaction of WO_2 in air.

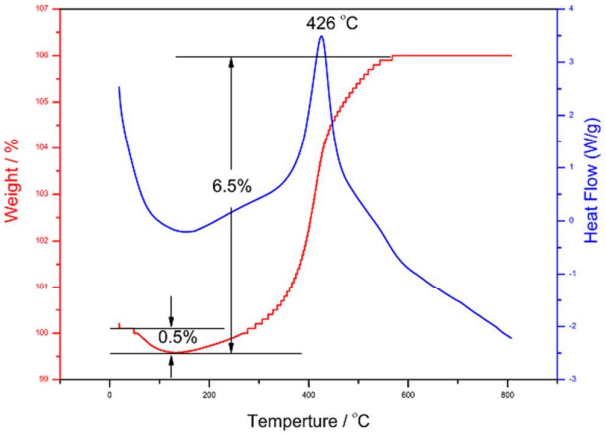

Fig. 2 TGA curve of WO_2/WO_3 sample in air flow

The XRD pattern of the WO_2/WO_3 microspheres (Figure 1b) exhibits that the diffraction intensity of WO_3 becomes weaker and WO_2 (JCPDS card no. 032-1393) characteristic peaks centred at 25.7°, 37.0° and 52.8° appear, indicating the formation of WO_2/WO_3 composite phases. The structure and morphology of the as-prepared samples were further characterized by SEM and TEM. It is found that WO_3 is gradually reduced due to homogeneous combination of oxygen atoms in the lattice with CO, without serious collapse and aggregation during the reduction process (Figure 3a). The as-prepared samples also show well-defined hollow spherical structures with an average diameter of ca. 3 um, as shown in the insert of Figure 3a. Furthermore, as shown in the HRTEM image (Figure 3c), the shell layers of microspheres (20 nm in thickness) show a lattice spacing of 0.34 nm and 0.24 nm consistent with the lattice orientation of (110) and (200) of WO_2. These results suggest that the WO_2/WO_3 sample manifests as a core-shell hierarchical structure. A feasible formation process for the WO_2/WO_3 microspheres under a CO/CO_2 atmosphere is as follows:

$WO_3 + CO \longrightarrow WO_2 + CO_2$ (2)

Platinum particles were loaded on the surface of WO_2/WO_3 microspheres by means of the conventional sodium borohydride reduction method. According to the HRTEM image (Figure 3d), the average platinum particle size is around 4-5 nm, which is in good agreement with the value calculated from XRD (Figure 1c) using the Debye-Scherrer equation (4.2 nm for Pt-WO_2/WO_3 catalyst).[11] Quantitative analysis of the EDS spectra of Pt-WO_2/WO_3 confirming the Pt loading concentration of 19.23%, which is close to actual loading amounts of Pt (Figure S3). The Elemental mapping images (Figure S4) show that the platinum particles are finely dispersed on the surface of the WO_2/WO_3 microspheres, which will provide a large number of interfaces as active sites for electrocatalytic reactions.

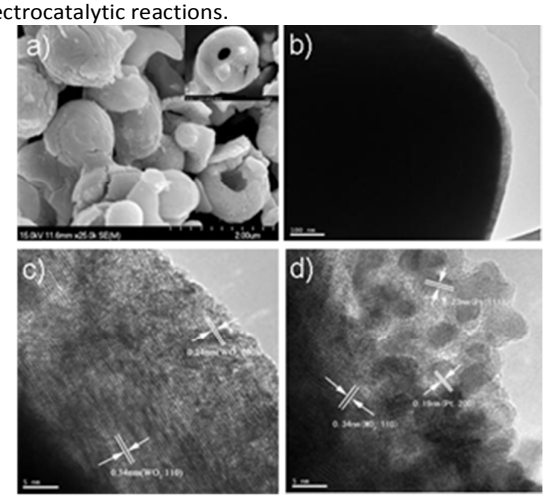

Fig. 3 a) SEM images of WO_2/WO_3; b,c) HRTEM images of WO_2/WO_3; d) TEM images of Pt-WO_2/WO_3

The cyclic voltammograms (CV) of h-WO_3 and WO_2/WO_3 supports were obtained in N_2-saturated H_2SO_4 solution at a sweep rate of 50 mV s^{-1}. The first-cycle CV curve of WO_2/WO_3 showed an oxidation peak centered at 0.71 V compared to CV curve of h-WO_3 (Figure S5a), which is probably attributed to the irreversible oxidation of the WO_2 shell into WO_3 species. The characteristic peak centered at 0.71 V disappeared in the following cycling, giving rise to a stable h-WO_3-like CV profile (Figure S5b). X-ray photoelectron spectroscopy (XPS) was also used in combination with CV to determine the surface oxidation states of W (Figure S6). Compared with two characteristic peaks for tungsten in the +Ⅵ oxidation state at 35.8 eV and 37.9 eV , the W4f spectrum of WO_2/WO_3 shows the negative shift, which probably arises from surface reduction of WO_3 in CO/CO_2 atmosphere.

The catalytic activities of Pt-WO_2/WO_3 catalyst towards the MOR were investigated in comparison with those of Pt/h-WO_3 and JM PtRu/C catalysts (Figure 4). For Pt-WO_3 catalysts, it is not suitable for employing the hydrogen underpotential deposition (H-UPD) measurements to calculate the Pt surface area because the intercalation of protons in WO_3 forming tungsten bronzes occur in the same potential region (−0.24 to 0.05 v) as H-UPD on Pt.[12] All the current density was consequently calculated by normalization to the mass of loaded Pt. As seen in the Figure 4a, the onset potential of methanol oxidation on Pt-WO_2/WO_3 is 50 mV more negative than that of JM PtRu/C and Pt/h-WO_3 catalysts, indicating that methanol oxidation can take place at a lower potential on Pt-WO_2/WO_3.[13] The mass specific current of Pt-WO_2/WO_3 (694 mA mg^{-1} Pt) is also the highest among three catalysts, which is 1.4 and 3.0 times of that of JM PtRu/C (506 mA mg^{-1} Pt) and

Pt/h-WO_3 (230 mA mg^{-1} Pt). Moreover, the I_f/I_b ratio (in which I_f and I_b are the forward and backward current densities, respectively) for Pt-WO_2/WO_3 (1.04) and JM PtRu/C (1.11) is higher than that of Pt/h-WO_3 (0.86), displaying that the Pt-WO_2/WO_3 has a better tolerance to carbonaceous species accumulation during the MOR.[14] The higher methanol oxidation current density of Pt-WO_2/WO_3 is further confirmed by Chronoamperometric curves (CA) recorded at 0.7 V for 6000 s (Figure 4b), which further verifies that Pt-WO_2/WO_3 exhibits better electrocatalytic stability in the MOR. Combined with the hydrogen spill-over effect and bifunctional mechanism,[15] the decrease of the electron-transfer resistance by the modification of WO_2 is responsible for the excellent electrocatalytic performance of Pt-WO_2/WO_3 catalyst.

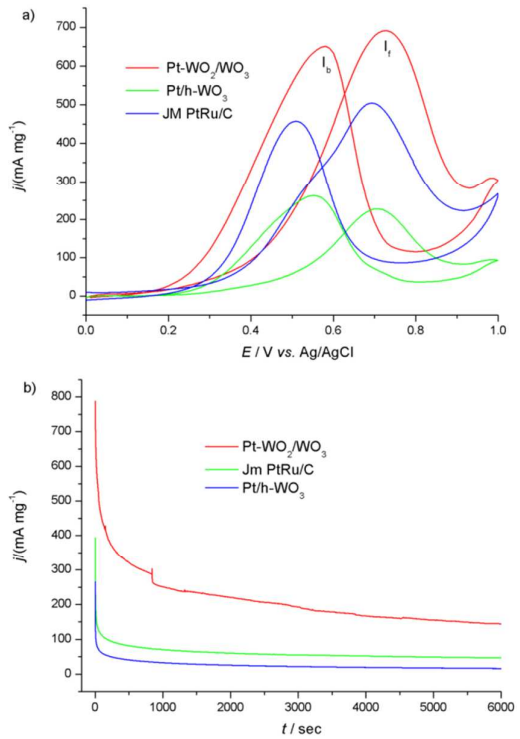

Fig. 4 a) Cyclic voltammetric curves of Pt-WO_2/WO_3, Pt/h-WO_3 and JM PtRu/C in 0.5 M H_2SO_4 + 1 M CH_3OH solution at the scan rate of 50 mV s^{-1}; Pt-WO_2/WO_3; b) Chronoamperometric curves of Pt-WO_2/WO_3, Pt/h-WO_3 and JM PtRu/C at 0.7 V for 6000s in 0.5 M H_2SO_4 + 1 M CH_3OH solution.

In summary, we have developed a novel method to synthesize WO_2/WO_3 with core-shell hierarchical structure. The as-prepared Pt-WO_2/WO_3 catalyst exhibits enhanced electrocatalytic activity in the MOR compared with JM PtRu/C and Pt/h-WO_3 catalysts. The synergetic combination of special core-shell structures and decrease of the electron-transfer resistance by the modification of WO_2 are mainly proposed to be responsible for the superior electrocatalytic activity of Pt-WO_2/WO_3 catalyst. The inherent characteristic of this core-shell structure may also make itself suitable for the applications in photocatalysis and gas sensors.

The research was financially supported by the Jiangxi Ganpo 555 Project for Excellent Talents, National Natural Science Foundation of China (No. 51404110) , Jiangxi Natural Science Foundation of China (No. 20151BAB213011) and the Postdoctoral Preferred Project Fund of Jiangxi Province (No. 2014zy15).

Notes and references

[a] School of Metallurgy and Chemical Engineering Jiangxi University of Science and Technology 86 Hongqi Road, Ganzhou 341000, PR China
E-mail: yangzhou1998@126.com
[b] Research Center of Analysis and Measurement Zhejiang University of Technology 18 Chaowang Road, Hangzhou 310032, PR China

Electronic Supplementary Information (ESI) available: Experimental details, SEM images of h-WO_3, EDS spectra and element mapping of Pt-WO_2/WO_3 catalysts, the CVs in acid solution and W4f XPS spectra of WO_3 and WO_2/WO_3, See DOI: 10.1039/c000000x/

1 (a) W. Wu, X. D. Xiang, Y. L. Lin and W. S. Li, *International Journal of Hydrogen Energy*, 2013, **38**, 11080; (b) Y. Liu, S. Shrestha and W. E. Mustain, *Acs Catalysis*, 2012, **2**, 456; (c) Z. G. Zhao, Z. J. Yao, J. Zhang, R. Zhu, Y. Jin and Q. W. Li, *J Mater Chem*, 2012, **22**, 16514; (d) A. Lewera, L. Timperman, A. Roguska and N. Alonso-Vante, *Journal of Physical Chemistry C*, 2011, **115**, 20153.
2 J. J. Wang, Z. Y. Wang and C. J. Liu, *Acs Applied Materials & Interfaces*, 2014, **6**, 12860.
3 X. Y. He, C. G. Hu, Q. N. Yi, X. Wang, H. Hua and X. Y. Li, *Journal of the Electrochemical Society*, 2013, **160**, F566.
4 X. C. Hu, Y. Zhou, H. R. Wen and H. M. Zhong, *Journal of the Electrochemical Society*, 2014, **161**, F583.
5 J. Zhang, J. P. Tu, G. H. Du, Z. M. Dong, Q. M. Su, D. Xie and X. L. Wang, *Electrochimica Acta*, 2013, **88**, 107.
6 Q. Wang, G. X. Wang, K. Sasaki, T. Takeguchi, T. Yamanaka, M. Sadakane and W. Ueda, *Journal of Power Sources*, 2013, **241**, 728.
7 R. Ganesan and J. S. Lee, *Journal of Power Sources*, 2006, **157**, 217.
8 A. Gulino, S. Parker, F. H. Jones and R. G. Egdell, *Journal of the Chemical Society-Faraday Transactions*, 1996, **92**, 2137.
9 S. X. Liu, H. B. Yin, H. B. Wang and J. C. He, *Journal of Alloys and Compounds*, 2013, **561**, 129.
10 Y. Zhou;, X. Hu;, Y. Xiao; and Q. Shu, *Electrochimica Acta*, 2013, **111**, 588.
11 R. Ganesan and J. S. Lee, *Angew Chem Int Edit*, 2005, **44**, 6557.
12 S. Jayaraman, T. F. Jaramillo, S. H. Baeck and E. W. McFarland, *Journal of Physical Chemistry B*, 2005, **109**, 22958.
13 (a) L. X. Ding, A. L. Wang, G. R. Li, Z. Q. Liu, W. X. Zhao, C. Y. Su and Y. X. Tong, *Journal of the American Chemical Society*, 2012, **134**, 5730; (b) H. Ataee-Esfahani, M. Imura and Y. Yamauchi, *Angew Chem Int Edit*, 2013, **52**, 13611.
14 (a) B. Y. Xia, H. B. Wu, X. Wang and X. W. Lou, *Journal of the American Chemical Society*, 2012, **134**, 13934; (b) H. H. Li, S. Zhao, M. Gong, C. H. Cui, D. He, H. W. Liang, L. Wu and S. H. Yu, *Angew Chem Int Edit*, 2013, **52**, 7472.
15 (a) F. Micoud, F. Maillard, A. Bonnefont, N. Job and M. Chatenet, *Physical Chemistry Chemical Physics*, 2010, **12**, 1182; (b) X. Z. Cui, J. L. Shi, H. R. Chen, L. X. Zhang, L. M. Guo, J. H. Gao and J. B. Li, *Journal of Physical Chemistry B*, 2008, **112**, 12024; (c) A. C. C. Tseung and K. Y. Chen, *Catalysis Today*, 1997, **38**, 439; (d) K. Y. Chen, P. K. Shen and A. C. C. Tseung, *Journal of the Electrochemical Society*, 1995, **142**, L54.